

AD-A220 868

REPORT SSD-TR-90-10

DTIC FILE COPY

Higher-Order Mode Dependencies in Gain-Guided Twin-Stripe Laser Diode Arrays

D. G. HEFLINGER, M. B. CHANG, and W. R. FENNER
Electronics Research Laboratory
Laboratory Operations
The Aerospace Corporation
El Segundo, CA 90245

27 February 1990

Prepared for

SPACE SYSTEMS DIVISION
AIR FORCE SYSTEMS COMMAND
Los Angeles Air Force Base
P.O. Box 92960
Los Angeles, CA 90009-2960


APPROVED FOR PUBLIC RELEASE;
DISTRIBUTION UNLIMITED

DTIC
ELECTE
APR 24 1990
S B D
Co

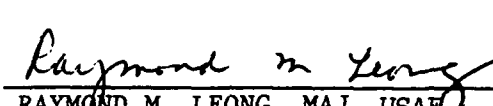
This report was submitted by The Aerospace Corporation, El Segundo, CA 90245, under Contract No. F04701-88-C-0089 with the Space Systems Division, P.O. Box 92960, Los Angeles, CA 90009-2960. It was reviewed and approved for The Aerospace Corporation by M. J. Daugherty, Director, Electronics Research Laboratory. Jane Cristoff was the project officer for the Mission-Oriented Investigation and Experimentation (MOIE) program.

This report has been reviewed by the Public Affairs Office (PAS) and is releasable to the National Technical Information Service (NTIS). At NTIS, it will be available to the general public, including foreign nationals.

This technical report has been reviewed and is approved for publication. Publication of this report does not constitute Air Force approval of the report's findings or conclusions. It is published only for the exchange and stimulation of ideas.



JANE CRISTOFF
MOIE Project Officer
SSD/CNDAS



RAYMOND M. LEONG, MAJ, USAF
MOIE Program Manager
AFSTC/WCO OL-AB

UNCLASSIFIED

SECURITY CLASSIFICATION OF THIS PAGE

REPORT DOCUMENTATION PAGE				
1a. REPORT SECURITY CLASSIFICATION Unclassified		1b. RESTRICTIVE MARKINGS		
2a. SECURITY CLASSIFICATION AUTHORITY		3. DISTRIBUTION/AVAILABILITY OF REPORT		
2b. DECLASSIFICATION/DOWNGRADING SCHEDULE		Approved for public release; distribution unlimited.		
4. PERFORMING ORGANIZATION REPORT NUMBER(S) TR-0088(3925-04)-3		5. MONITORING ORGANIZATION REPORT NUMBER(S) SSD-TR-90-10		
6a. NAME OF PERFORMING ORGANIZATION The Aerospace Corporation Laboratory Operations		6b. OFFICE SYMBOL (if applicable)	7a. NAME OF MONITORING ORGANIZATION Space Systems Division	
6c. ADDRESS (City, State, and ZIP Code) El Segundo, CA 90245-4691		7b. ADDRESS (City, State, and ZIP Code) Los Angeles Air Force Base Los Angeles, CA 90009-2960		
8a. NAME OF FUNDING/SPONSORING ORGANIZATION		8b. OFFICE SYMBOL (if applicable)	9. PROCUREMENT INSTRUMENT IDENTIFICATION NUMBER F04701-88-C-0089	
8c. ADDRESS (City, State, and ZIP Code)		10. SOURCE OF FUNDING NUMBERS		
		PROGRAM ELEMENT NO.	PROJECT NO.	TASK NO.
				WORK UNIT ACCESSION NO.
11. TITLE (Include Security Classification) Higher-Order Dependencies in Gain-Guided Twin-Stripe Laser Diode Arrays				
12. PERSONAL AUTHOR(S) Heflinger, Donald G.; Chang, Michael B.; and Fenner, Wayne R.				
13a. TYPE OF REPORT		13b. TIME COVERED FROM _____ TO _____	14. DATE OF REPORT (Year, Month, Day) 1990 February 27	15. PAGE COUNT 31
16. SUPPLEMENTARY NOTATION.				
17. COSATI CODES		18. SUBJECT TERMS (Continue on reverse if necessary and identify by block number)		
FIELD	GROUP	SUB-GROUP	Laser diode; Gain guided; Array	
			Supermode; Index guided; Near field	
			Higher order mode; Twin stripe; Far field	
			Spectrally resolved near-field; Two stripe.	
19. ABSTRACT (Continue on reverse if necessary and identify by block number) Experimental data and modeling are presented which show that under appropriate conditions a set of index-guided modes can exist and have lower thresholds than gain-guided supermodes for twin-stripe semiconductor lasers. It is also shown that more than the two modes predicted by supermode theory can simultaneously lase. The near-field and far-field profiles of the index-guided modes will be shown to have a narrower extent than those predicted by supermode theory and, in the case of the fundamental mode, be single-lobed. <i>1/24/90</i>				
20. DISTRIBUTION/AVAILABILITY OF ABSTRACT <input checked="" type="checkbox"/> UNCLASSIFIED/UNLIMITED <input type="checkbox"/> SAME AS RPT. <input type="checkbox"/> DTIC USERS		21. ABSTRACT SECURITY CLASSIFICATION Unclassified		
22a. NAME OF RESPONSIBLE INDIVIDUAL		22b. TELEPHONE (Include Area Code)	22c. OFFICE SYMBOL	

PREFACE

The authors gratefully acknowledge Markus Van Loan and Richard D. Reel for assistance in the fabrication and testing of the laser diodes used in this work. Professor Elsa M. Garmire reviewed the original manuscript and provided helpful comments.

Accession For	
NTIS GRA&I	<input checked="" type="checkbox"/>
DTIC TAB	<input type="checkbox"/>
Unannounced	<input type="checkbox"/>
Justification	
By _____	
Distribution/	
Availability Codes	
Dist	Avail and/or Special
A-1	

CONTENTS

PREFACE.....	1
I. INTRODUCTION.....	7
II. EXPERIMENT.....	9
III. ANALYTICAL MODEL.....	11
A. Gain-Guided Modes.....	15
B. Gain-Guided Supermode.....	16
C. Index-Guided Mode.....	16
Table 1. Constants Used in Model Calculations.....	13
IV. RESULTS.....	19
V. CONCLUSIONS.....	31
REFERENCES.....	33

FIGURES

1.	(a) Layer Structure and Stripe Geometry of the Twin-Stripe DH Laser. (b) Current Density Distribution in the Active Layer. (c) Real Index Profile in the Active Layer.....	12
2.	Facet Images of Schottky-Barrier-Defined Stripe Lasers.....	20
3.	Near-field Intensity Profiles Experimentally Measured from a Single-Stripe Gain-Guided Laser and from a Twin-Stripe Laser with a Center-to-Center Stripe Separation of 8 μm for the Fundamental Mode and the First Order Mode.....	21
4.	Calculated Near-Field Intensity Profiles of the Out-of-Phase Gain-Guided Supermode with an Effective Current Width $W = 4 \mu\text{m}$ and Center-to-Center Stripe Separation $2S = 8 \mu\text{m}$ at a Current Density of $J_0 = 1800 \text{ A/cm}^2$	22
5.	Spectrally Resolved Near-Field Images of Twin-Stripe Lasers with Increasing Center-to-Center Stripe Separations.....	24
6.	Far-Field Intensity Profiles for an 8- μm Center-to-Center Stripe Separation.....	25
7.	Experimentally Measured Near-Field Intensity Profile of a Laser with 18- μm Center-to-Center Stripe Separation and the Calculated Profile for the Index-Guided Fourth Order Mode.....	27
8.	Experimental Far-Field Intensity Profile from a Laser with an 18- μm Center-to-Center Stripe Separation and the Calculated Far-Field Intensity Profile Computed from the Index-Guided Fourth Order Mode Depicted in Fig. 7.....	28
9.	Effect of Stripe Separation Upon the Threshold Currents and Threshold Current Densities.....	29

TABLE

1.	Constants Used in Model Calculations.....	13
----	---	----

I. INTRODUCTION

Multiple-stripe semiconductor lasers are of current interest as a means of achieving higher power. Due to the relative simplicity of both material growth and device fabrication, many of these devices are made from planar double heterostructure (DH) material. In an attempt to better understand multiple-stripe DH lasers, we have studied the simplest example -- the twin-stripe laser diode.

A single-stripe device made from planar DH material, with the stripe defined by etching through a dielectric layer, operates in a gain-guided mode. The current that is injected into a stripe produces a gain profile that is peaked under the stripe. A secondary effect is a lowering of the refractive index to form an antiwaveguide. For a single-stripe laser, the gain is sufficiently strong to overcome the losses due to the antiwaveguide, resulting in the familiar gain-guided laser modes. Multiple-stripe devices have been thought to operate as coherently coupled arrays of gain-guided stripes in which the output modes are linear combinations of the gain-guided modes from the individual stripes -- the so-called "supermodes." In this case, the field profiles of individual stripes are peaked beneath the stripes. Because the index profile is antiguiding, the field is leaky and couples to other stripes via propagating waves [1]. However, it is known that the supermode model fails to predict some experimentally observed modes in multistripe arrays [2-6]. Recently, experimental data [7] have shown that the mode with the lowest threshold in a twin-stripe DH laser is an index-guided mode located between the stripes. This mode has less gain than the supermode, but also has considerably less loss. Its existence has also been known for some time [8]. However, the index-guided modes have apparently been overlooked until recently [5-7] as modes of laser arrays.

Both the near- and far-field lateral intensity profiles from a twin-stripe array are initially single-lobed [7]. At a higher drive current, an

additional two-lobed lateral mode is observed. Although it was initially thought that this higher order mode was the out-of-phase supermode, we will show that it, along with other modes to be presented in this report, is part of a family of index-guided modes. We will show that the index-guided modes can have lasing thresholds less than the gain-guided supermodes, that the mode order of the index-guided modes will increase as the stripe separation is increased, and that the mode with the lowest threshold is the highest order mode allowed by the guide. In addition, as the injection current (and gain) is increased, the height of the index-guide increases, allowing even higher order modes to exist. These higher order modes will lase due to the large overlap between the gain and the intensity. Thus, the mode order will increase as the injection current increases.

The experimental measurements and data which qualitatively support the presence of index-guided modes are described in section II. An analytic model and its assumptions are described in detail in section III. Quantitative experimental data and comparisons with calculations are presented in section IV, while section V summarizes our findings.

II. EXPERIMENT

Single- and twin-stripe laser diodes were fabricated from double heterostructure (DH) material grown by metal-organic chemical vapor deposition. Stripe contacts were defined using a 4- μm mask either with a Si_3N_4 insulation layer or a reverse-biased Schottky barrier contact. The Schottky barrier was formed by etching through the heavily doped GaAs cap layer to the lighter doped p-isolation layer and uniformly evaporating metal over the wafer. The stripe width of the Schottky-barrier-defined devices was reduced to 3 μm by the etching process. Both the Si_3N_4 and the Schottky-barrier devices behaved similarly, as did devices fabricated from different wafers, indicating that their performance was independent of the fabrication technique and that ridge waveguiding did not occur in the Schottky-barrier devices. The Si_3N_4 devices and the Schottky barrier devices were typically pulsed with 100-ns pulses at a 1-kHz repetition rate. The Schottky barrier devices were also tested CW.

One advantage of using a reverse-biased Schottky barrier to define the stripes for this study was that the position of the stripes could be determined from the etch profile. Photographs of the facets were made which simultaneously showed both the location of the stripe and the emitted light.

Spectrally resolved near-field images were obtained by focusing the facet (with the diode junction aligned parallel to the entrance slit) on a monochromator and placing a solid-state video camera in the plane of the exit slit [7]. Near-field intensity profiles were obtained by digitizing linescans of the spectrally resolved near-field images. Far-field intensity profiles were measured by scanning a slit across the output beam.

III. ANALYTICAL MODEL

The optical field profile, $E(x,y)$, is calculated by solving the transverse wave equation,

$$\nabla_t^2 E(x,y) + (k_0^2 \epsilon - \beta^2) E(x,y) = 0 \quad (1)$$

where $\nabla_t^2 = \partial^2/\partial x^2 + \partial^2/\partial y^2$, \hat{x} is the direction normal to the junction, \hat{y} is the direction parallel to the junction, β is the longitudinal wavevector, k_0 is the freespace wavevector ($2\pi/\lambda_0$), and ϵ is the complex dielectric constant which includes the gain, distributed losses, and the real refractive indices. The gain can be changed by varying the injected current. The threshold current density is calculated by equating the modal gain, which is proportional to the imaginary part of the longitudinal wavevector, β , to the Fabry-Perot reflection losses at the facets. Two different solutions to the wave equation were considered for the geometry of interest: supermodes created by coherently combining two gain-guided modes located under the stripes, and an index-guided mode located between the stripes.

The planar double heterostructure (DH) layer structure and two-stripe contact geometry of the stripes are shown in Fig. 1(a). In terms of the complex refractive index, the dielectric constant is given by

$$\epsilon + \Delta\epsilon \approx n^2 + 2n_a \nabla n \quad (2)$$

$$n = n_r + i\alpha/2k_0 \quad (3a)$$

$$\nabla n = -g_{\text{bulk}} (b + i)/2k_0 \quad (3b)$$

$$g_{\text{bulk}} = -g_s (J/d - J_1) \quad (3c)$$

where n (the complex refractive index with no injected current) changes with the epitaxial layers but is independent of y . In the active layer, n

TYPICAL CURRENT
SPREADING UNDER
A STRIPE

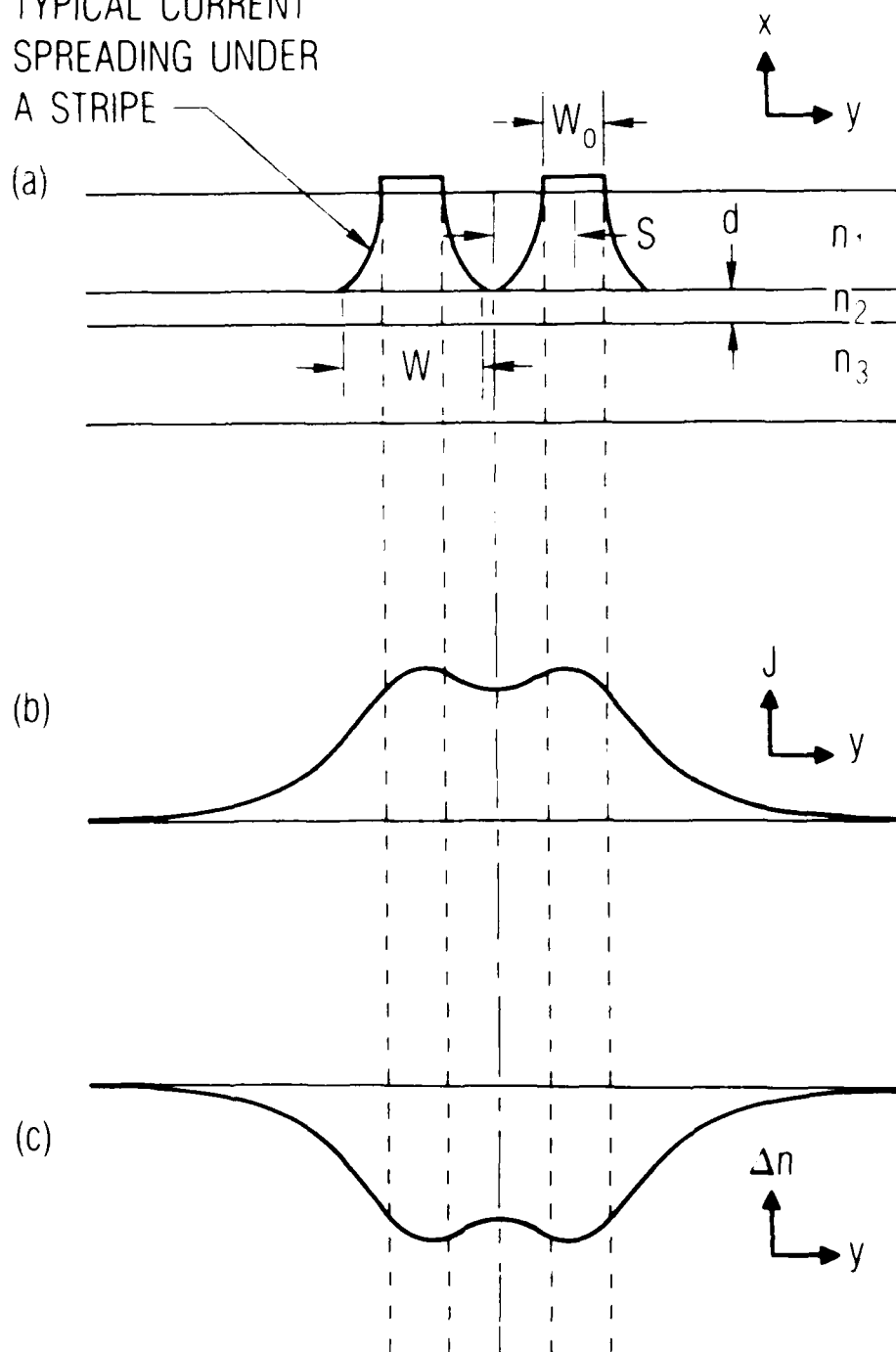


Fig. 1. (a) Layer Structure and Stripe Geometry of the Twin-Stripe DH Laser. (b) Current Density Distribution in the Active Layer. (c) Real Index Profile in the Active Layer.

is denoted by n_a . The real refractive index with no injected current, n_r , is also dependent upon the epitaxial layer. The loss coefficient for the optical intensity, α , is equivalent to negative bulk gain. The change in the complex refractive index due to the injected current, which is nonzero only in the active layer, is denoted by Δn and is a function of the lateral dimension, y , through the bulk gain, g_{bulk} , which in turn is a linear function of the injected current [8,9]. The injected current density is J , while J_1 and g_s are material parameters and d is the thickness of the active layer. The parameter b is the ratio between the real and imaginary parts of n implied by experimental data [10]. Streifer's value of $b = 3$ is used in these calculations. The device and material parameters used in this report are summarized in Table 1. A large value of b will result in a large change in the real refractive index under the stripes, which will result in a lossier gain-guided supermode with a larger threshold and a more tightly confined index-guided mode with a lower threshold.

Table 1. Constants Used in Model Calculations.

<u>Device Parameter</u>	<u>Value</u>	
λ_0	815.0 nm	
n_1	3.39	
n_2	3.565	
n_3	3.39	
d	0.1 μm	
L	250 μm	
S	4 μm	
<u>Material Parameter</u>	<u>Value</u>	<u>Reference</u>
g_s	1/24 cm^2/A	8
J_1	4000/24	8
b	3	10

The injected current density profile in the active layer is assumed, for simplicity in modeling, to have the form $\text{sech}^2(y)$ with equal current injection at each stripe [10]:

$$J(y) = J_0 \{ \text{sech}^2[(y - S)/W] + \text{sech}^2[(y + S)/W] \} \quad (4)$$

where $2S$ is the center-to-center stripe spacing and W is the effective width of the current distribution. The current density profile is shown in Fig. 1(b). Note that current spreading should make W slightly larger than the stripe width W_0 . Integration of this profile leads to a total current of $I = 4LWJ_0$. The gain profile is proportional to the current profile. The real part of the index profile given by (3b) with a current distribution given by (4) is plotted in Fig. 1(c), showing the index-guiding region which occurs between the stripes and the antiguiding region which occurs beneath the stripes.

The current density, in the region between the stripes where y is small, can be approximated by

$$J(y) = c_1 + c_2 y^2 \quad (5a)$$

where

$$c_1 = 2J_0 [2 - \tanh^2(S/W)] \quad (5b)$$

$$c_2 = 2(J_0/W^2)[-1 + 4 \tanh^2(S/W) - 3 \tanh^4(S/W)] \quad (5c)$$

For the parameters of interest, c_2 is positive so that the current density profile between the stripes is a concave-up parabola and the resultant real index profile is a guiding concave-down parabola. This parabolic current density profile allows calculation of index-guided modes with analytic mode profiles.

Substituting (2) and (3) into (1) results in a differential equation that is dependent upon the injected current. This equation has analytical solutions for current profiles given by either (4) or (5). The modal gain, which is proportional to the imaginary part of the longitudinal wavevector, β , is determined using the method of weighted indices [11]. Solving for the modal gain and equating it to the reflective losses, results in the threshold condition for lasing.

The longitudinal wavevector is obtained by premultiplying (1) with $E^*(x,y)$ and integrating over the (x,y) plane.

$$\beta^2 = \int E^*(x,y) (\nabla_t^2 + k_0^2 \epsilon) E(x,y) dx dy \quad (6a)$$

$$= \langle E | \nabla_t^2 + k_0^2 \epsilon | E \rangle \quad (6b)$$

The method of weighted indices [11] assumes that the transverse field can be separated:

$$E(x,y) = X(x)Y(y) \quad (7)$$

A. GAIN-GUIDED MODES

The gain-guided mode of a single-stripe array can be modeled by assuming a current density of the form $\text{sech}^2(y)$. This leads to a solution of the wave equation with the form [10]

$$Y(y) = \cosh \mu [(y - y_1)/W] \quad (8a)$$

where

$$\mu(\mu + 1) = -n_a(b + i)g_s J_0 k_0 W^2 / d \quad (8b)$$

This is the lowest order mode of a family of modes. However, this is the only one of interest in the present study. Solving for the single-stripe longitudinal wavevector, β , using the method of weighted indices [11], yields

$$\beta^2 = - \langle E | \partial^2 / \partial x^2 | E \rangle + k_0^2 \langle E | n^2 | E \rangle + \Gamma k_0 n_a J_1 b g_s + (1/W)^2 \quad (9a)$$

where

$$\Gamma = \int_0^d E^*(x) E(x) dx \quad (9b)$$

B. GAIN-GUIDED SUPERMODE

Linear superposition of the gain-guided single-stripe modes, justified by coupled mode theory, is used to determine the modes of the two-stripe gain-guided device:

$$Y(y) = a_1 Y_1(y - y_1) + a_2 Y_2(y - y_2) \quad (10)$$

We assume that both stripes are equally pumped, $Y_1(y) = Y_2(y)$. Then, substitution of (10) into the wave equation and using (8a) to define $Y(y)$ results in two solutions for a_1 and a_2 : an in-phase solution, $a_1 = a_2$, and an out-of-phase solution, $a_1 = -a_2$.

The out-of-phase supermode has a lower threshold than the in-phase supermode so that, for the rest of this report, the former is the mode we will refer to as the gain-guided supermode. Supermodes constructed of higher-order single-stripe modes have even higher thresholds.

C. INDEX-GUIDED MODE

The only region in which index guiding can occur is between the stripes at $y = 0$. Approximating the current distribution between the stripes, using (5a) and substituting into (2) and (3), leads to a dielectric profile with a quadratic dielectric dependence. The solution of the wave equation is a Hermite-Gaussian [12],

$$Y_m(y) = Y_{om} \exp[-(ay)^2/2] H_m(ay) \quad (11)$$

where

$$a = [-g_s c_2 J_0 (b + i) n_a k_0 / d]^{1/4} \quad (12a)$$

$$Y_{om} = (a/p^{1/2} m! 2^m)^{1/2} \quad (12b)$$

and $H_m(ay)$ is the Hermite polynomial of order m . The field exponent, a , is dependent upon the injected current. As the current is increased, the field becomes more tightly confined and the full width at half maximum (FWHM) decreases. The longitudinal wavevector, β , is computed by substituting the lateral and transverse field dependencies in the wave equation and integrating over the (x,y) plane, resulting in

$$\beta^2 = - \langle E | \partial^2 / \partial x^2 | E \rangle + k_0^2 \langle E | n^2 | E \rangle \quad (13)$$

$$- (b+i) n_a k_0 g_s (c_1 J_0 / d - J_1) \Gamma - k_0 a.$$

The threshold condition is again obtained by equating the modal gain obtained from (13) to the reflective losses.

IV. RESULTS

Twenty-two twin-stripe laser diodes were chosen out of an initial set of thirty-five, after screening for facet inclusions and high thresholds (currents greater than 200 mA). These diodes were studied in depth by measuring the current threshold of each lateral mode, the spectrally resolved near-field intensity profile of each lateral mode, and the far-field intensity profile at various currents.

Images of the facets of several diodes just above lasing threshold are shown in Fig. 2. Figure 2(a) shows the near-field intensity distribution of a single-stripe laser, while Figs. 2(b) through 2(d) show the near-field distributions of twin-stripe devices of increasing stripe separation. The lateral mode of the single-stripe laser is single-lobed and has an extent considerably larger than the stripe width, indicative of the antiguiding inherent in a gain-guided device. On the left-hand side of Fig. 3(a), the corresponding experimental (short dashes) and calculated (long and short dashes) intensity profiles are shown. The model parameters were selected to give good agreement between the experimental and calculated curves. These same model parameters, shown in Table 1, were then used in all subsequent calculations.

The image of the mode with the lowest threshold current in a twin-stripe laser with center-to-center stripe separation of 8 μm is shown in Fig. 2(b). In contrast with the single stripe, the mode is narrow and confined to the region between the stripes. There is good agreement between the experimental (dashed) and calculated (solid) intensity profiles shown on the right-hand side of Fig. 3(a). The corresponding near-field intensity profile for the out-of-phase supermode is shown in Fig. 4. The multilobed near-field intensity is a result of interference between the two gain-guided fields [1] which extend well beyond the stripe boundaries. As the current is increased, the profiles narrow and the locations of the intensity peaks move together. None of these characteristics agree with the experimental observations.

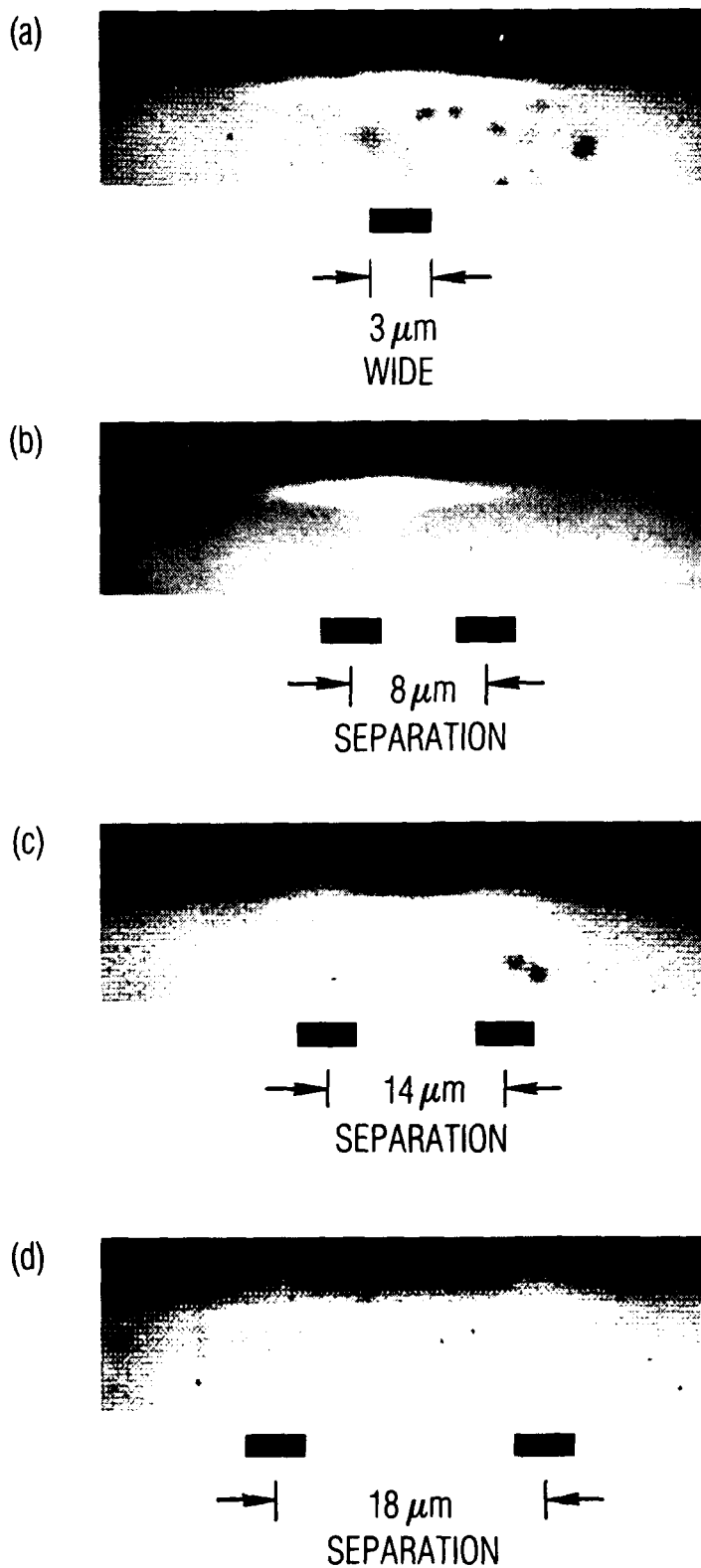


Fig. 2. Facet Images of Schottky-Barrier-Defined Stripe Lasers. (a) Single-stripe laser. (b)-(d) Twin-stripe lasers with center-to-center stripe separations.

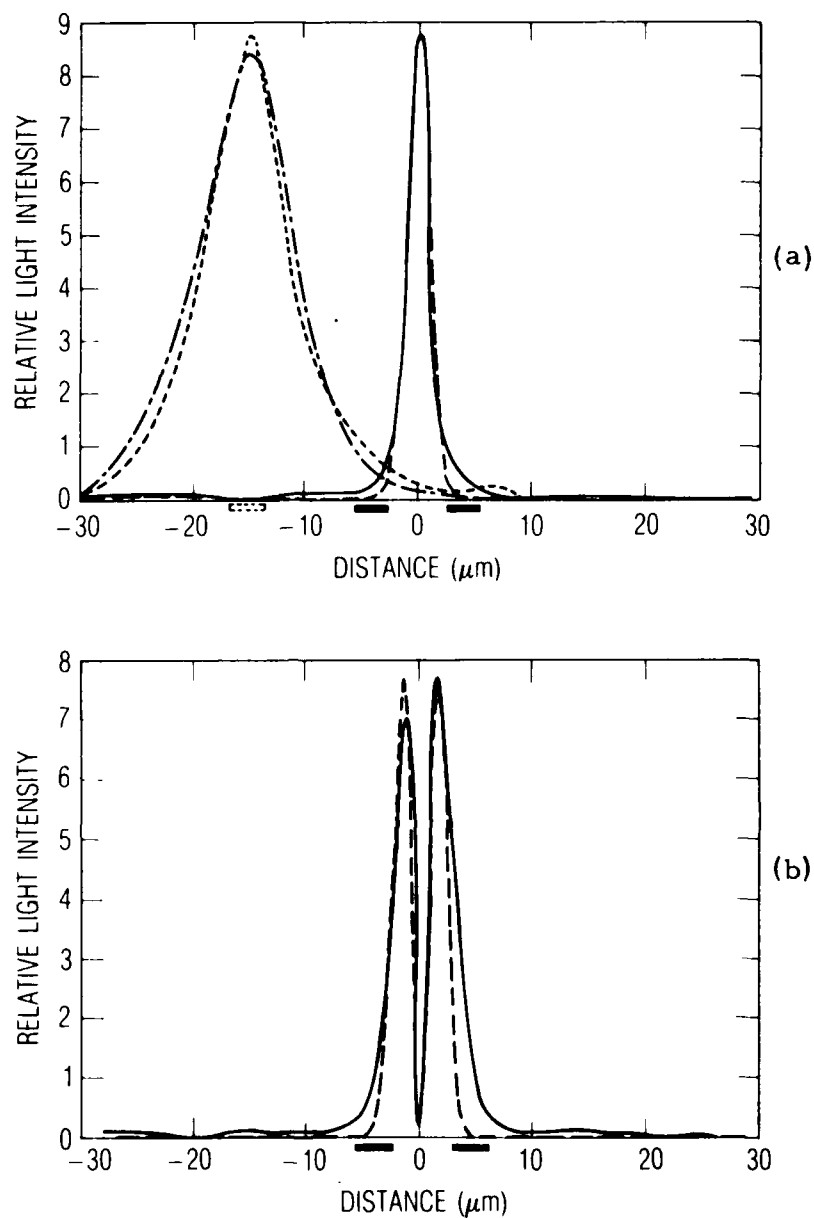


Fig. 3. Near-field Intensity Profiles Experimentally Measured from a Single-Stripe Gain-Guided Laser (dotted curve) and from a Twin-Stripe Laser with a Center-to-Center Stripe Separation of $8 \mu\text{m}$ (solid curves) for (a) the Fundamental Mode and (b) the First Order Mode. The calculated near-field profiles for the single-stripe laser and the fundamental and first order modes of the twin-stripe laser are shown by the dot-dash curve and the dashed curves, respectively. The fundamental mode was measured at a current in which only the fundamental mode existed.

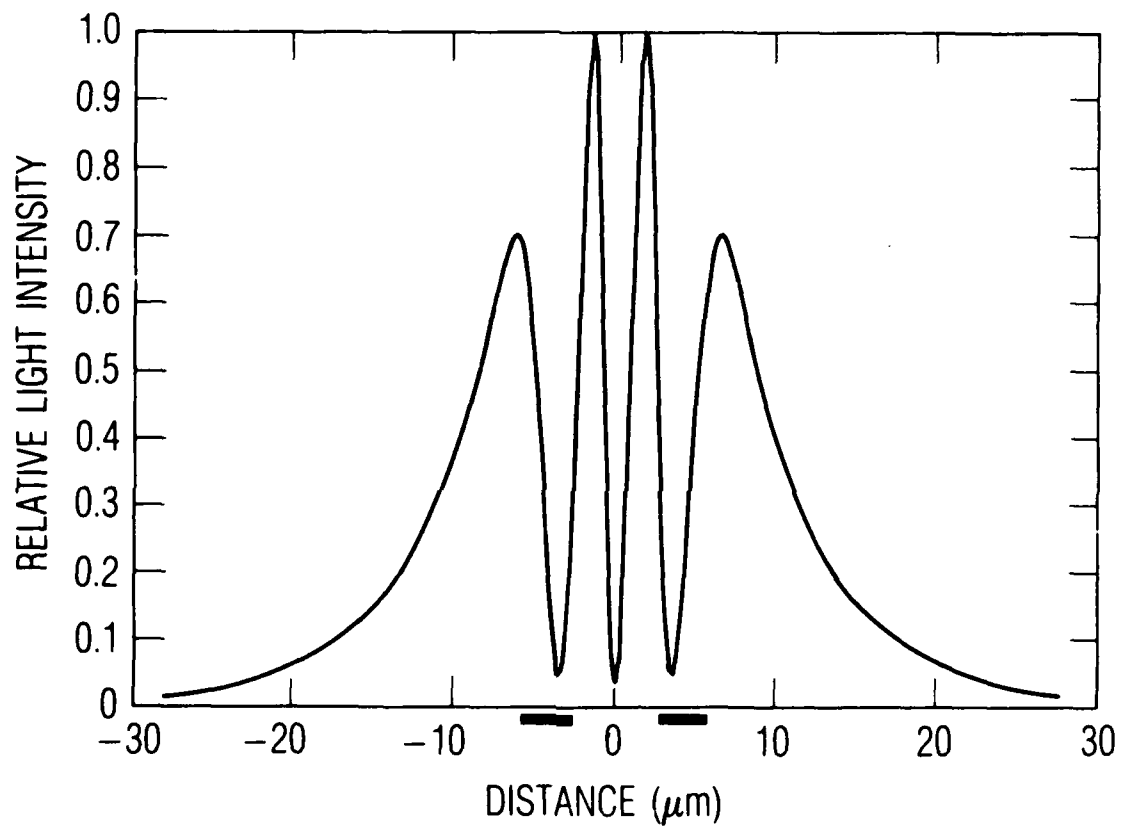


Fig. 4. Calculated Near-Field Intensity Profiles of the Out-of-Phase Gain-Guided Supermode with an Effective Current Width $W = 4 \mu\text{m}$ and Center-to-Center Stripe Separation $2S = 8 \mu\text{m}$ at a Current Density of $J_0 = 1800 \text{ A/cm}^2$.

At higher currents, a second and third mode were observed. This is evident in the spectrally resolved near-field image shown in Fig. 5(a). The single-lobed mode at the longest wavelength appeared first, followed by the double- and then the triple-lobed modes. It is tempting to attribute the double-lobed mode to the out-of-phase supermode [7]. However, note that the extent of the pattern is still well within the outer boundaries of the stripes. Calculated (dashed) and experimental (solid) intensity profiles for the double-lobed mode are shown in Fig. 3(b). The calculated profile assumed the first order ($m = 1$) of the index-guided modes. In general, the shape and peak positions of the experimental and calculated profiles remained the same as the current was increased. For those modes near cut-off, the calculated peaks were slightly narrower than the experimental ones, probably due to the assumption of a parabolic index-guide.

The far-field intensity profile for the twin-stripe device with an 8- μm center-to-center stripe separation is shown in Fig. 6(a). The solid curve is experimental, while the dashed curve is calculated using the index-guided field profile. For comparison, the corresponding far-field pattern calculated for the out-of-phase supermode is shown in Fig. 6(b).

The effect of increasing the stripe separation on the near-field intensity patterns is shown in Figs. 2(c), 2(d), and 5(b) through 5(f). Figures 2(c) and 2(d) are images of the first modes to lase and indicate that higher-order modes are favored as the stripe separation increases. This is because the gain profile, which is peaked under the stripes, is a better match to the highest allowed mode profile. Again we note that the light is fairly well confined between the stripes and does not appreciably extend beyond the outer edges of the two stripes, even for the largest stripe separation measured. The spectrally resolved near-field images shown in Figs. 5(b) through 5(f) show the existence of several modes at currents above lasing threshold. The longest wavelength mode lases first, with higher-order modes at shorter wavelengths appearing as the current is increased. The fact that higher-order modes lase at higher currents is understood by noting that the depth of the index-guide increases with increasing current, thereby permitting the higher-order modes to exist.

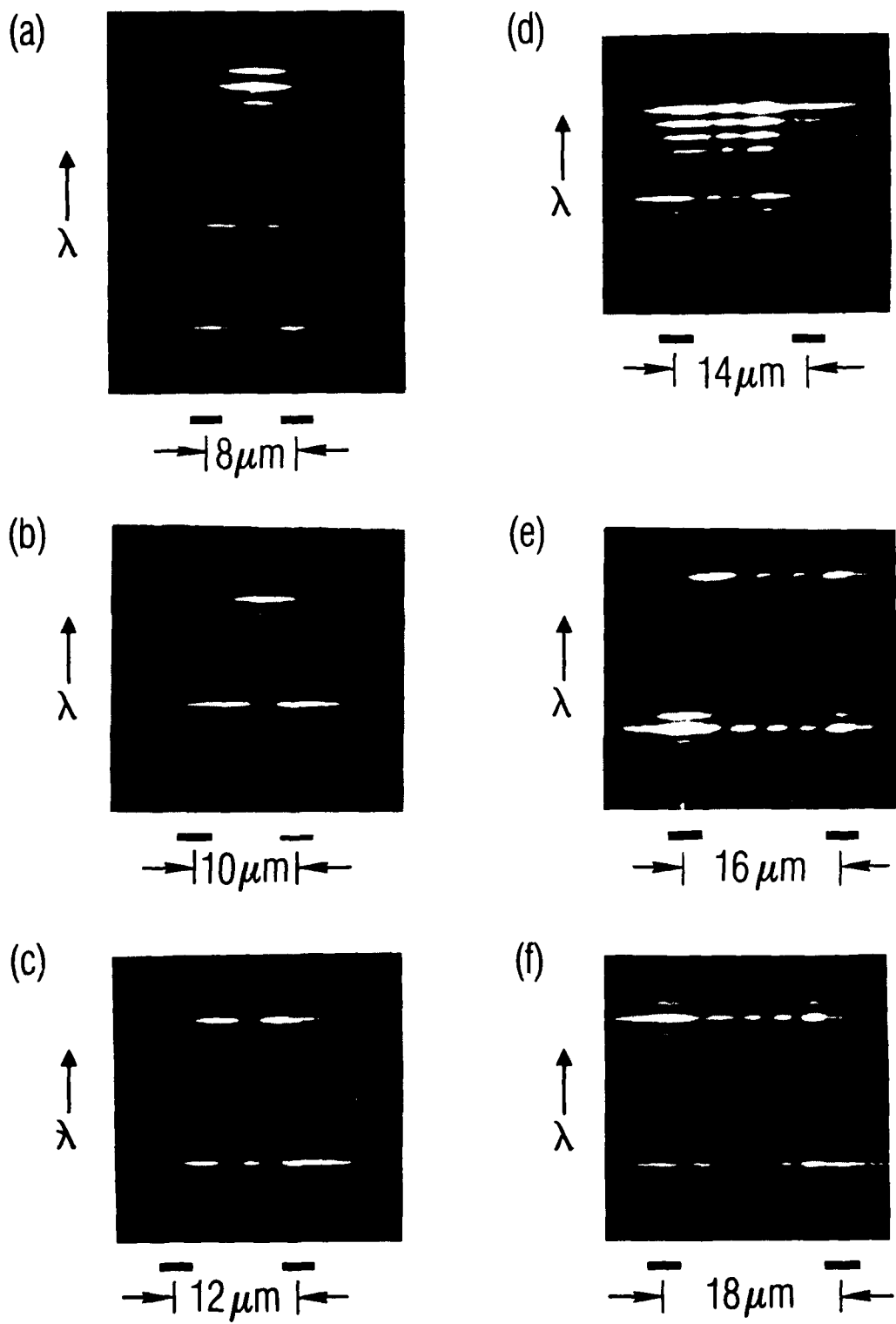


Fig. 5. Spectrally Resolved Near-Field Images of Twin-Stripe Lasers with Increasing Center-to-Center Stripe Separations

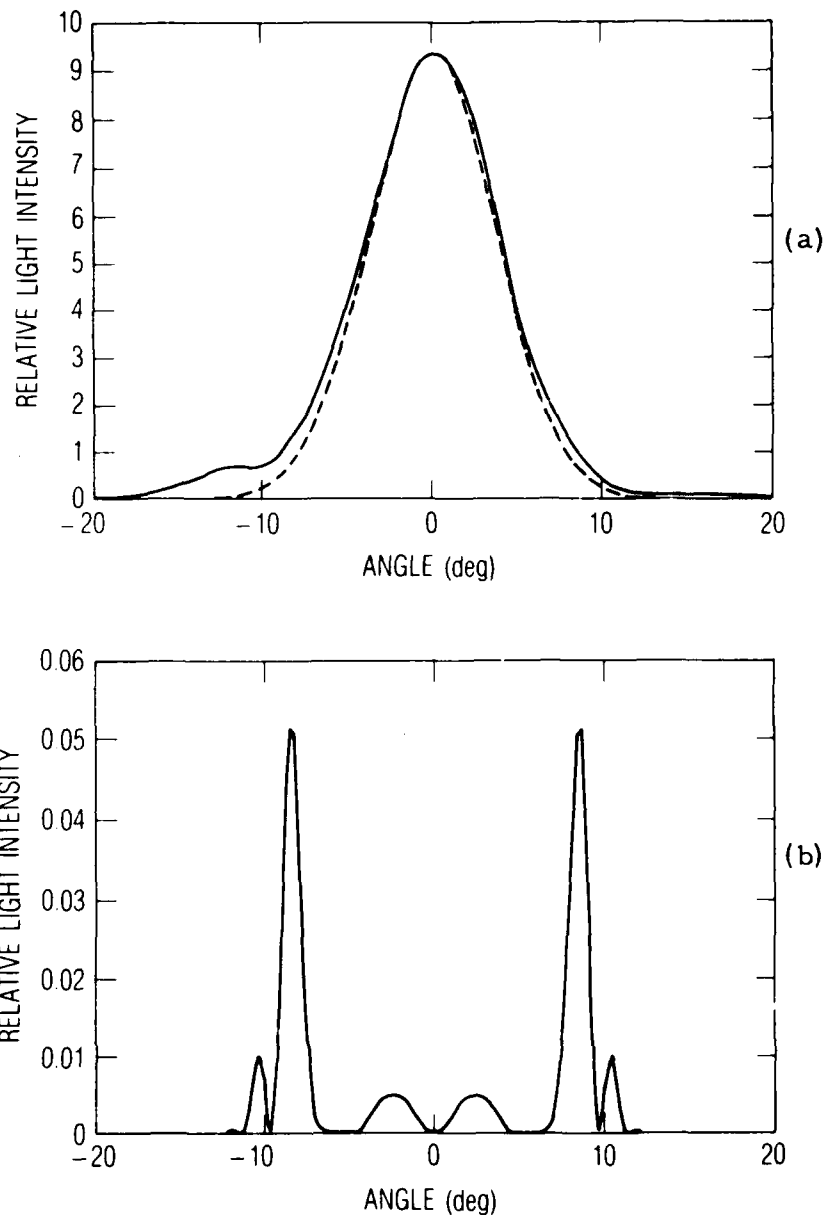


Fig. 6. Far-Field Intensity Profiles for an 8- μm Center-to-Center Stripe Separation. (a) The experimentally measured far-field intensity profile (solid curve) at the same current as in Fig. 3(a) and the calculated far-field intensity profile (dashed curve) assuming the near-field profile shown in Fig. 3(a). (b) Calculated far-field intensity profiles of the out-of-phase gain-guided supermode for the near-field intensity depicted in Fig. 4, $J_0 = 1800 \text{ A/cm}^2$.

The experimental (solid) and calculated (dashed) near- and far-field intensity profiles for a stripe separation of $18 \mu\text{m}$ are shown in Figs. 7 and 8, respectively. The experimental results and the curves calculated from the index-guided model are in reasonable agreement.

The experimentally measured threshold currents of each lateral mode supported by the twenty-two twin-stripe lasers are plotted as a function of stripe separation in Fig. 9(a). All the lasers studied supported at least two modes, and several supported three modes within the current range of 0 to 200 mA. The threshold current densities computed for the four lowest index-guided modes are shown plotted versus stripe separation in Fig. 9(b). In all cases, the effective width of the single-stripe current distribution, W , was taken to be $4 \mu\text{m}$. The current threshold for the gain-guided supermode is shown as a dashed line. It is constant because of the weak coupling assumption. For small stripe separations, the dip in the current profile assumed by the model disappears and no index-guided modes can exist. For each higher mode, the model predicts a minimum in the threshold current as a function of stripe separation. For large values of S , the threshold increases due to the increasing mismatch between the gain and mode profiles. The situation is less clear at small values of S . A given mode can only exist above a certain value of current. As S decreases, that current increases as does the gain. The point at which the mode can exist already has excess gain over loss at small values of S , i.e., it is not possible to predict where the modal gain and reflective loss are equal since the gain always exceeds the loss when the modes appear.

We see that there is some qualitative agreement between the experimental and calculated values. The factors in agreement as the stripe separation is increased are the general increase in threshold current and the increase in mode order of the mode with the lowest threshold current. However, the model and experimental data are not in good agreement regarding which modes should appear as the current increases. The lack of agreement is probably due to a number of factors -- the assumption of an infinite parabolic index profile between the stripes which affects the relative magnitude of the slopes on either side of the minima, the fact

that several of the device and material parameters are not known precisely, and the fact that the model is based on a cold cavity calculation utilizing modes of an infinite waveguide.

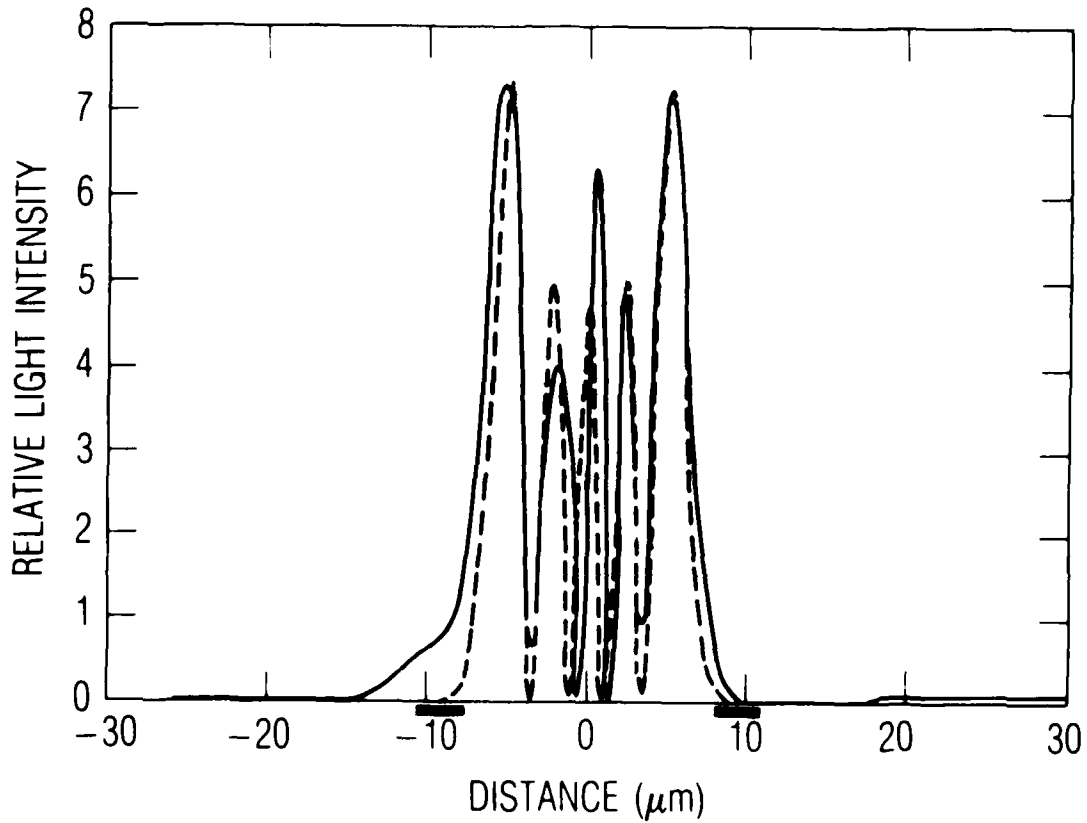


Fig. 7. Experimentally Measured Near-Field Intensity Profile (solid curve) of a Laser with 18- μm Center-to-Center Stripe Separation and the Calculated Profile for the Index-Guided Fourth Order Mode (dashed curve).

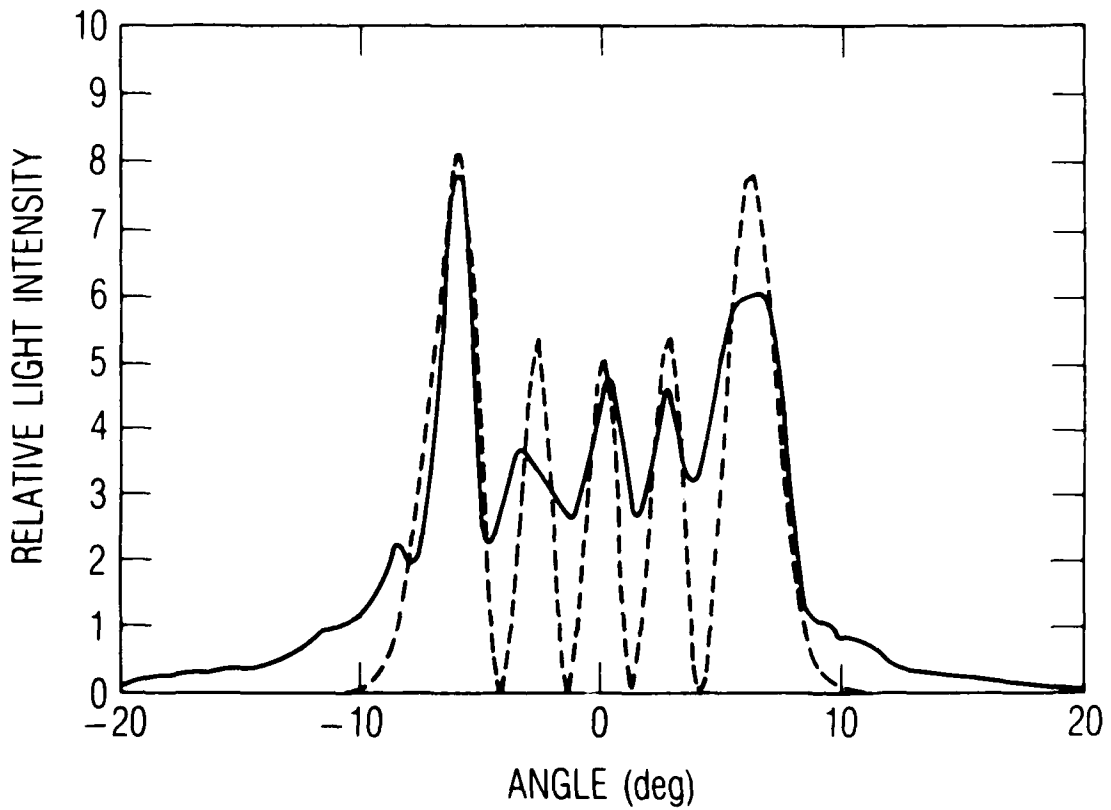


Fig. 8. Experimental Far-Field Intensity Profile (solid curve) from a Laser with an 18- μm Center-to-Center Stripe Separation and the Calculated Far-Field Intensity Profile (dashed line) Computed from the Index-Guided Fourth Order Mode Depicted in Fig. 7.

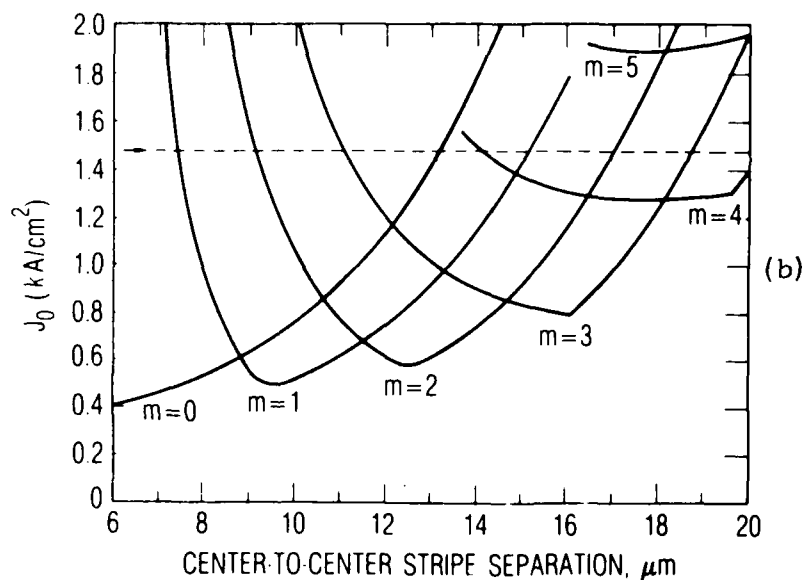
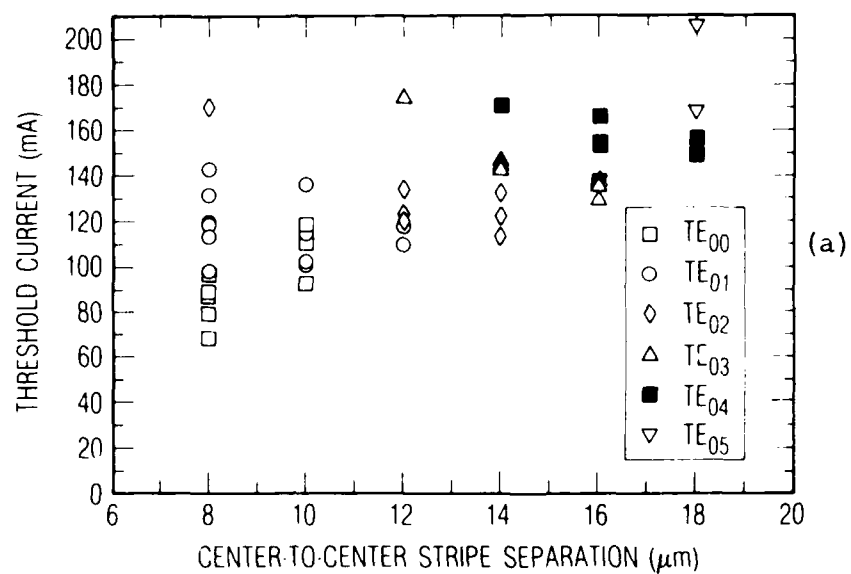


Fig. 9. Effect of Stripe Separation Upon the Threshold Currents and Threshold Current Densities. (a) The measured threshold currents of the different lateral modes. (b) The calculated threshold current densities for the index-guided modes (solid curve) and the gain-guided supermode (dashed curve) assuming an effective current width of $W = 4 \mu\text{m}$.

V. CONCLUSIONS

Data and analysis have been presented which clearly show that laser diodes fabricated as closely spaced arrays of stripes in double hetero-structure material operate in a family of index-guided modes. The order of the lateral modes increases with both the injected current and the stripe separation, and several modes can simultaneously lase. These observations are supported by a model which assumes that a real index guide, formed by the dip in the current profile, exists between the stripes. We have used a quadratic fit to calculate the resulting lateral modes. The lowest order mode is single-lobed in both the near- and far-field. (The in-phase gain-guided supermode would also have a single-lobe far-field but the threshold of that mode is much higher than other modes and was not seen.)

The existence of these index-guided modes may prove significant in arrays of more than two stripes. In a multistripe array, the index-guided fundamental modes formed between the stripes may couple and lock together. Because of the large gain between these fundamental modes, i.e., under the stripes, in-phase operation is expected [13]. Preliminary experiments on three-stripe laser arrays with center-to-center spacings of 8 μm are consistent with the existence of index-guided modes which appear to be coupled in-phase.

REFERENCES

1. E. Kapon, C. Lindsey, J. Katz, S. Margalit, and A. Yariv, "Coupling mechanism of gain-guided integrated semiconductor laser arrays," Appl. Phys. Lett. 44, 389-391 (1984).
2. J. P. Hohimer, G. R. Hadley, and A. Owyong, "Interelement coupling in gain-guided diode laser arrays," Appl. Phys. Lett. 48, 1504-1506 (1986).
3. G. R. Hadley, J. P. Hohimer, and A. Owyong, "High-order ($m > 10$) eigenmodes in ten-stripe gain-guided diode laser arrays," Appl. Phys. Lett. 49, 684-686 (1986).
4. W. K. Marshall and J. Katz, "Direct analysis of gain-guided phase-locked semiconductor laser arrays," J. Quantum Electron. QE-22, 827-832 (1986).
5. J. Buus, "'Excess' modes in gain-guided laser arrays," Electron. Lett. 22, 1296-1297 (1986).
6. D. Mehuys and A. Yariv, "Coupled-wave theory of multiple-stripe semiconductor injection lasers," Opt. Lett. 13, 571-573 (1988).
7. D. G. Heflinger and W. R. Fenner, "Simultaneous operation of gain- and index-guided lateral modes in twin-stripe laser diode arrays," J. Appl. Phys., 64, 3750-3751 (1988).
8. G. H. B. Thompson, Physics of Semiconductor Laser Devices, John Wiley & Sons, New York, 1980.
9. H. Kressel and J. K. Butler, Semiconductor Lasers and Heterojunction LEDs, Academic Press, Inc., San Diego, 1977.
10. W. Streifer, R. D. Burnham, and D. R. Scifres, "Symmetrical and asymmetrical waveguiding in very narrow conducting stripe lasers," IEEE J. Quantum Electron. QE-15, 136-141 (1979).
11. P. C. Kendall, M. J. Adams, S. Ritchie, and M. J. Robertson, "Theory for calculating approximate values for the propagation constants of an optical rib waveguide by weighting the refractive indices," IEE Proc. 134(A), 699-702 (1987).
12. F. Stern, "Gain-current relation for GaAs lasers with n-type and undoped active layers," IEEE J. Quantum Electron. QE-9, 290-294 (1973).

13. L. Figueroa, T. L. Holcomb, K. Burghard, D. Bullock, C. B. Morrison, L. M. Zinkiewicz, and G. A. Evans, "Modeling of the optical characteristics for twin-channel laser (TCL) structures," IEEE J. Quantum Electron. QE-22, 2141-2149 (1986).

LABORATORY OPERATIONS

The Aerospace Corporation functions as an "architect-engineer" for national security projects, specializing in advanced military space systems. Providing research support, the corporation's Laboratory Operations conducts experimental and theoretical investigations that focus on the application of scientific and technical advances to such systems. Vital to the success of these investigations is the technical staff's wide-ranging expertise and its ability to stay current with new developments. This expertise is enhanced by a research program aimed at dealing with the many problems associated with rapidly evolving space systems. Contributing their capabilities to the research effort are these individual laboratories:

Aerophysics Laboratory: Launch vehicle and reentry fluid mechanics, heat transfer and flight dynamics; chemical and electric propulsion, propellant chemistry, chemical dynamics, environmental chemistry, trace detection; spacecraft structural mechanics, contamination, thermal and structural control; high temperature thermomechanics, gas kinetics and radiation; cw and pulsed chemical and excimer laser development, including chemical kinetics, spectroscopy, optical resonators, beam control, atmospheric propagation, laser effects and countermeasures.

Chemistry and Physics Laboratory: Atmospheric chemical reactions, atmospheric optics, light scattering, state-specific chemical reactions and radiative signatures of missile plumes, sensor out-of-field-of-view rejection, applied laser spectroscopy, laser chemistry, laser optoelectronics, solar cell physics, battery electrochemistry, space vacuum and radiation effects on materials, lubrication and surface phenomena, thermionic emission, photosensitive materials and detectors, atomic frequency standards, and environmental chemistry.

Electronics Research Laboratory: Microelectronics, solid-state device physics, compound semiconductors, radiation hardening; electro-optics, quantum electronics, solid-state lasers, optical propagation and communications; microwave semiconductor devices, microwave/millimeter wave measurements, diagnostics and radiometry, microwave/millimeter wave thermionic devices; atomic time and frequency standards; antennas, rf systems, electromagnetic propagation phenomena, space communication systems.

Materials Sciences Laboratory: Development of new materials: metals, alloys, ceramics, polymers and their composites, and new forms of carbon; nondestructive evaluation, component failure analysis and reliability; fracture mechanics and stress corrosion; analysis and evaluation of materials at cryogenic and elevated temperatures as well as in space and enemy-induced environments.

Space Sciences Laboratory: Magnetospheric, auroral and cosmic ray physics, wave-particle interactions, magnetospheric plasma waves; atmospheric and ionospheric physics, density and composition of the upper atmosphere, remote sensing using atmospheric radiation; solar physics, infrared astronomy, infrared signature analysis; effects of solar activity, magnetic storms and nuclear explosions on the earth's atmosphere, ionosphere and magnetosphere; effects of electromagnetic and particulate radiations on space systems; space instrumentation.